High-Rayleigh-number convection in a fluid-saturated porous layer

By JESSE OTERO[1], LUBOMIRA A. DONTCHEVA[2],
HANS JOHNSTON[3], RODNEY A. WORTHING[4],
ALEXANDER KURGANOV[5], GUERGANA PETROVA[6]
AND CHARLES R. DOERING[3,7]

[1]Department of Mathematics, Ohio State University, Columbus, OH 43210, USA

[2]Department of Computer Science & Engineering, University of Washington, Seattle,
WA 98195-2350, USA

[3]Department of Mathematics, University of Michigan, Ann Arbor, MI 48109-1109, USA

[4]Breasco LLC, Ann Arbor, MI 48197, USA

[5]Department of Mathematics, Tulane University, New Orleans, LA 70118, USA

[6]Department of Mathematics, Texas A&M University, College Station, TX 77843-3368, USA

[7]Michigan Center for Theoretical Physics, Ann Arbor, MI 48109-1120, USA

The Darcy–Boussinesq equations at infinite Darcy–Prandtl number are used to study convection and heat transport in a basic model of porous-medium convection over a broad range of Rayleigh number Ra. High-resolution direct numerical simulations are performed to explore the modes of convection and measure the heat transport, i.e. the Nusselt number Nu, from onset at $Ra = 4\pi^2$ up to $Ra = 10^4$. Over an intermediate range of increasing Rayleigh numbers, the simulations display the 'classical' heat transport $Nu \sim Ra$ scaling. As the Rayleigh number is increased beyond $Ra = 1255$, we observe a sharp crossover to a form fitted by $Nu \approx 0.0174 \times Ra^{0.9}$ over nearly a decade up to the highest Ra. New rigorous upper bounds on the high-Rayleigh-number heat transport are derived, quantitatively improving the most recent available results. The upper bounds are of the classical scaling form with an explicit prefactor: $Nu \leqslant 0.0297 \times Ra$. The bounds are compared directly to the results of the simulations. We also report various dynamical transitions for intermediate values of Ra, including hysteretic effects observed in the simulations as the Rayleigh number is decreased from 1255 back down to onset.

1. Introduction

Buoyancy-driven flows such as thermal convection are of great importance for a wide range of phenomena in geophysical, astrophysical and engineering applications. Rayleigh–Bénard convection in particular is a fundamental paradigm for nonlinear dynamics including instabilities and bifurcations, pattern formation, chaotic dynamics and developed turbulence (Kadanoff 2001). Despite the great deal of attention that has been devoted to it, the dynamics of high-Rayleigh-number (Ra) convective turbulence and the associated enhancement of the heat transport (represented by the Nusselt number Nu) still present challenges for theory and experiment.

At the time of writing there are still a number of questions regarding the Nu–Ra relationship in fluids presumed to be well-described by the Boussinesq equations.

There, just beyond onset the classical marginally stable boundary layer argument predicts a $Nu \sim Ra^{1/3}$ 'soft turbulent' scaling (Howard 1964). At higher Rayleigh numbers a so-called 'hard turbulence' regime sets in along with the appearance of a large-scale flow and the data are better fitted by a $Ra^{2/7}$ scaling (Heslot, Castaing & Libchaber 1987). Recent experiments over an extremely large range of Rayleigh numbers report an exponent closer to 0.31, a value between the soft and hard exponents (Niemela *et al.* 2000). On the other hand, high-precision experiments over a more limited range of Ra have called into question the validity of the scaling hypothesis altogether (Xu, Bajaj & Ahlers 2000), although this may be explained by crossovers among different scaling regimes (Grossmann & Lohse 2000). The longstanding theoretical conjecture of a $Nu \sim Ra^{1/2}$ 'ultimate' asymptotic scaling by Kraichnan (1962) and Spiegel (1971) has been proven to be the upper limit for scaling in the basic model (Howard 1963; Busse 1969; Doering & Constantin 1996; Nicodemus, Grossmann & Holthaus 1998; Otero *et al.* 2002; Plasting & Kerswell 2003), but the experimental data are currently considered controversial and do not constitute a conclusive consensus (Chavanne *et al.* 1997; Glazier *et al.* 1999; Sommeria 1999). Moreover, fully developed turbulent convection in simple fluids described by the Boussinesq equations is still sufficiently complex dynamically that direct numerical simulations lag well behind experiments in terms of the magnitude of Rayleigh numbers that can be achieved (Kerr & Herring 2000). Even in the infinite-Prandtl-number limit of the Boussinesq equations, where Navier–Stokes dynamics are replaced by the linear Stokes equations, unresolved mathematical challenges remain (Chan 1971; Constantin & Doering 1999; Doering & Constantin 2001; Otero 2002).

In this paper we focus on what may be the simplest dynamical setting for Rayleigh–Bénard convection, flow in a fluid-saturated porous layer modelled by the Darcy–Oberbeck–Boussinesq equations in the infinite Darcy–Prandtl number limit. This system distills the physics of convection down to a 'minimal' coupling of the heat advection–diffusion equation to Darcy's equation for the incompressible flow field via a simple buoyancy force. Our aim is to push outward the computational and rigorous analytical limits of what is known about the complex nonlinear dynamics that the interplay of these basic mechanisms (buoyancy and incompressibility) can produce. We study this simple model in order to better understand both the physics of these processes and the technical mathematical tools at our disposal.

Porous-media convection is of interest for a variety of geological and engineering applications, and this particular model has proven to be a useful quantitative model over a range of Rayleigh numbers (Nield & Bejan 1992). Its dynamics and bifurcation structure have been thoroughly explored theoretically and computationally for low-to-intermediate Rayleigh numbers both for the standard Rayleigh–Bénard problem studied here (Graham & Steen 1994), and more recently for an open-top version of the problem (Cherkaoui & Wilcock 1999). For any real application, however, this model is expected to break down at sufficiently high Rayleigh numbers when length scales in the flow and temperature fields shrink down to the pore length scale in the medium (Lister 1990); beyond that a quadratic drag law should replace Darcy's Law for the flow (Nield & Joseph 1985). Furthermore, it is likely that there is a practical limit to the magnitude of the Rayleigh numbers that may be explored for this model in the laboratory (Shattuck *et al.* 1997). This is because the higher the Rayleigh number is pushed, the smaller the pore scales must be for the model to remain valid, which means the slower the convection evolves so that even in well-controlled experiments inevitable extraneous heat losses, interruptions, and finite lifetimes of the experimenters themselves would undoubtedly conspire to frustrate

reliable long-term measurements of stationary-state dynamics. Nevertheless, from a purely theoretical viewpoint the mathematical and computational simplicity of this model makes it an attractive system to explore in the high-Rayleigh-number limit. Indeed, well-controlled 'numerical experiments' on this system can produce highly resolved simulations providing reliable insights into the nonlinear dynamics and data for comparison with theory and mathematical analysis.

The rest of this paper is organized as follows: In §2 we set out the details of the model and present some basic definitions. In §3 we describe the numerical methods and present the results of the simulations. Section 4 contains the derivation of improved rigorous upper bounds for the heat transport as a function of the Rayleigh number. The concluding §5 is a brief summary and discussion of the results, including a comparison of the rigorous bounds with the data from the numerical experiments.

2. Statement of the problem

We consider a layer of fluid-saturated porous material confined between two horizontal plates at $z = 0$, $z = 1$. The temperature field $T(\boldsymbol{x}, t)$, the velocity field $\boldsymbol{u}(\boldsymbol{x}, t) = \hat{\boldsymbol{i}}u + \hat{\boldsymbol{j}}v + \hat{\boldsymbol{k}}w$, and the pressure $P(\boldsymbol{x}, t)$ evolve according to

$$T_t + \boldsymbol{u} \cdot \nabla T = \Delta T, \tag{2.1}$$

$$\nabla \cdot \boldsymbol{u} = 0, \tag{2.2}$$

$$\boldsymbol{u} + \nabla P = \hat{\boldsymbol{k}} Ra\, T. \tag{2.3}$$

This model is obtained from the Darcy–Oberbeck–Boussinesq equations after non-dimensionalizing and taking the infinite Prandtl–Darcy number limit (Nield & Bejan 1992). Only one dimensionless parameter, the Rayleigh number

$$Ra = \frac{g\alpha(T_{bot} - T_{top})Kh}{\nu\kappa}, \tag{2.4}$$

remains. The various quantities in this Rayleigh number are the acceleration due to gravity g in the vertical (z) direction, the thermal expansion coefficient of the fluid α, the temperature drop across the plates $T_{bot} - T_{top}$, the Darcy permeability coefficient K (the square of a small pore length scale characterizing the medium), the height of the layer h, and the diffusivity constants for momentum ν and heat κ. The non-dimensional temperature of the bottom and top plates is held fixed at 1 and 0, respectively. We impose periodic boundary conditions on all the dynamical variables in the horizontal (x and y) directions and, because fluid is not allowed through the plates, $w\big|_{z=0,1} = 0$.

Our goal is to observe, from direct numerical simulations, and estimate, from first principles via rigorous upper bounds, the bulk-averaged vertical heat transport as measured by the Nusselt number

$$Nu = \left\langle \frac{1}{A} \int (\boldsymbol{u}T - \nabla T) \cdot \hat{\boldsymbol{k}} \right\rangle = 1 + \frac{1}{A} \left\langle \int wT \right\rangle, \tag{2.5}$$

in terms of the Rayleigh number. In (2.5), A is the (non-dimensional) area of the plates, $\int f$ denotes a volume integral over the entire fluid layer, and the angle brackets indicate the long-time average

$$\langle f \rangle = \lim_{T \to \infty} \frac{1}{T} \int_0^T f(t)\, \mathrm{d}t \tag{2.6}$$

(presuming, as we will for the purposes of this study, that these long-time limits exist).

From the equations of motion it is straightforward to derive equivalent expressions for the Nusselt number,

$$Nu = -\frac{1}{A}\left\langle \int_{z=0} \frac{\partial T}{\partial z}\,dx\,dy \right\rangle = -\frac{1}{A}\left\langle \int_{z=1} \frac{\partial T}{\partial z}\,dx\,dy \right\rangle = \frac{1}{A}\langle \|\nabla T\|^2 \rangle, \qquad (2.7)$$

where $\|f\| = (\int |f|^2)^{1/2}$.

3. Numerical simulations

We compute two-dimensional numerical solutions of the model equations (2.1), (2.2), (2.3), dropping the y-dependence of all variables and setting $v = 0$. As a matter of convenience, we recast the problem using the deviation of the temperature field from the conduction solution, $\Theta = T - (1 - z)$, and the stream function ψ where $(u, w) = (-\psi_z, \psi_x)$. The boundary conditions for these new variables are

$$\Theta\big|_{z=0,1} = 0 \quad \text{and} \quad \psi_x\big|_{z=0,1} = 0. \qquad (3.1)$$

The equations of motion are then

$$\Theta_t + \nabla \cdot (\boldsymbol{u}\Theta) - w = \Delta\Theta, \qquad (3.2)$$

$$\Delta\psi = Ra\,\Theta_x. \qquad (3.3)$$

The numerical method we use for approximating (3.2)–(3.3) is a spatially fourth-order finite difference scheme, second order in time, on a grid with spacings Δx and Δz in x and z, respectively. Denote by $\widetilde{\mathrm{D}}$ and D^2 standard second-order centred finite difference approximations of ∂ and ∂^2, respectively. First, (3.2) is formally discretized spatially using fourth-order compact operators as

$$\Theta_t + \left(\frac{\widetilde{\mathrm{D}}_x}{1 + \frac{1}{6}(\Delta x)^2 \mathrm{D}_x^2}(u\Theta) + \frac{\widetilde{\mathrm{D}}_z}{1 + \frac{1}{6}(\Delta z)^2 \mathrm{D}_z^2}(w\Theta) - w \right)$$
$$= \left(\frac{\mathrm{D}_x^2}{1 + \frac{1}{12}(\Delta x)^2 \mathrm{D}_x^2} + \frac{\mathrm{D}_z^2}{1 + \frac{1}{12}(\Delta z)^2 \mathrm{D}_z^2} \right) \Theta. \quad (3.4)$$

Then multiply through by the common denominator of the operators in the diffusion term, using the fact that $(1 + (\Delta x)^2 \mathrm{D}_x^2/6)^{-1} = (1 - (\Delta x)^2 \mathrm{D}_x^2/6) + O(h^4)$ – and similarly for the third term in (3.4) – and simplify. Incompressibility gives $\widetilde{\mathrm{D}}_x(u\Theta) + \widetilde{\mathrm{D}}_z(w\Theta) = u\widetilde{\mathrm{D}}_x\Theta + w\widetilde{\mathrm{D}}_z\Theta + O(h^2)$, which is used in order to avoid one-sided approximations in the convection term near the boundaries. Then discarding all terms involving $O(h^4)$ gives the desired implementable fourth-order discretization.

For the time discretization, in order to avoid any stability constraint due to the $O(1)$ diffusion coefficient, the diffusion term is treated implicitly using Crank–Nicholson, while the convection term (including $-w$) is discretized via the second-order explicit Adams–Bashforth scheme. The result is a discrete Poisson-like equation for computing Θ^{n+1} given (Θ^n, u^n, w^n) and $(\Theta^{n-1}, u^{n-1}, w^{n-1})$, which is solved using FFT-based methods with Dirichlet boundary condition $\Theta\big|_{z=0,1} = 0$ and periodic boundary conditions in x. Stability requires

$$\Delta t \leqslant \frac{h}{\|\boldsymbol{u}\|_\infty} = \text{CFL} \leqslant 1,$$

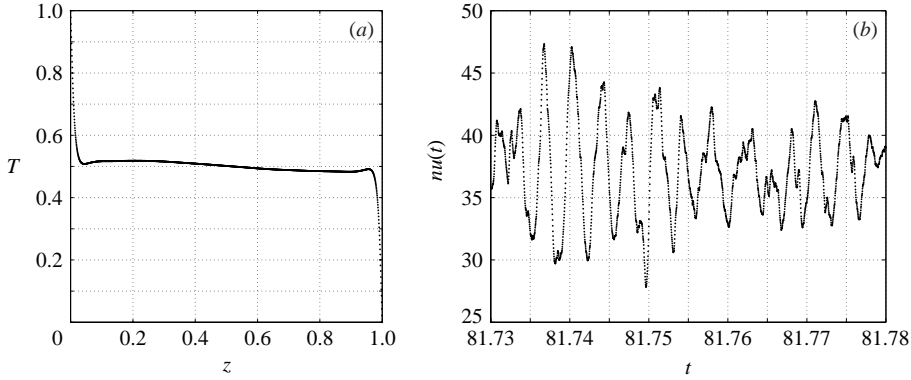where Δt is the time step and $h = \min\{\Delta x, \Delta z\}$.

FIGURE 1. (a) Horizontally averaged and time-averaged vertical temperature profile at $Ra = 5000$. The individual data points show the high spatial resolution. (b) Time series of the bulk averaged instantaneous heat flux $nu(t) = 1 + (1/A) \int w(\cdot, t) T(\cdot, t)$ at $Ra = 5000$. The individual data points shown are spaced more than 100 time steps Δt apart, illustrating the fine temporal resolution.

Next, a fourth-order discretization of (3.3) is given by

$$\left(\frac{D_x^2}{1 + \frac{1}{12}(\Delta x)^2 D_x^2} + \frac{D_z^2}{1 + \frac{1}{12}(\Delta z)^2 D_z^2} \right) \psi = Ra \widetilde{D}_x \left(1 - \frac{(\Delta x)^2}{6} D_x^2 \right) \Theta. \qquad (3.5)$$

Thus given Θ^{n+1} we solve this discrete Poisson equation for ψ^{n+1} with Dirichlet boundary conditions $\psi|_{z=0,1} = 0$ and periodic boundaries in x, again using FFT-based methods. Lastly, $\boldsymbol{u}^{n+1}$ is recovered from ψ^{n+1} via $(u, w) = (-\psi_z, \psi_x)$ using the fourth-order long-stencil approximations

$$u = -\widetilde{D}_z \left(1 - \frac{(\Delta z)^2}{6} D_z^2 \right) \psi \quad \text{and} \quad w = \widetilde{D}_x \left(1 - \frac{(\Delta x)^2}{6} D_x^2 \right) \psi. \qquad (3.6)$$

Note that the first equation in (3.6) requires values of ψ at two computational points outside of the domain along the boundaries. These are consistently prescribed by noting that (3.3) and (3.1) imply that $\psi_{zz} = 0$ along the boundaries. Both a one-sided and centred fourth-order discretization is applied to this, from which the required values are derived.

The protocol for our numerical experiments was to begin just above $Ra_c = 4\pi^2 \approx 39.5$ and step-by-step increase the Rayleigh number by a constant factor, allowing the flow to settle into a stationary dynamical state – a steady, periodic, or statistically stationary chaotic (turbulent) state – at each stage before increasing Ra further. After this 'run' to high Ra, another such run was made from high Rayleigh numbers back down to onset, decreasing Ra by a constant factor and allowing relaxation at each step, to explore hysteretic effects in the dynamics.

Specifically, simulations were performed starting from a small perturbation of the conduction state at Rayleigh number of $Ra = 50$ on a cell of size $[0, 2] \times [0, 1]$. After it was determined that the flow had reached a statistical steady state, Ra was increased by a multiple factor of $10^{1/10}$. At each stage we take $\delta = 15 Ra^{-1}$ as a conservative approximation of the thermal boundary layer thickness, and the grid resolution $\Delta x = \Delta z$ is chosen to ensure that approximately five grid points fell within the thermal boundary layer. In fact we over-resolve the flow in space and time to ensure the reliability of the results. To illustrate this, in figure 1(a) we show plots
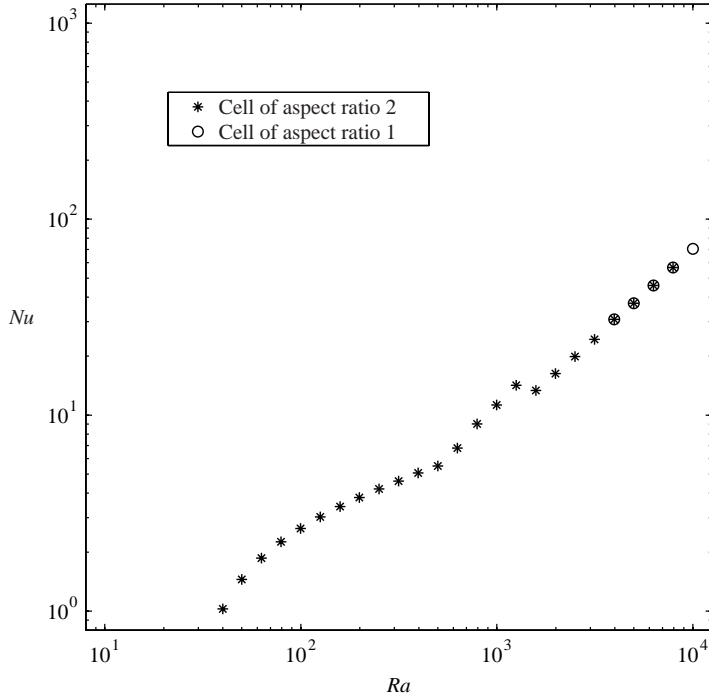
FIGURE 2. Plot of *Nu* vs. *Ra* data for the increasing-*Ra* run. The asterisks indicate the data from simulations in a cell of aspect ratio 2, the circle at the highest *Ra* is from a cell of aspect ratio 1, and the circled-asterisk data points were measured for both aspect ratio 1 and 2 with no discernible difference in *Nu* .

of the horizontally averaged and time-averaged vertical temperature profile and in figure 1(*b*) a time series of the bulk-averaged instantaneous heat flux $nu(t) = 1 + (1/A) \int w(\cdot, t) T(\cdot, t)$ at Rayleigh number $Ra = 5000$. The data in the profile plot show the spatial resolution, and the data points shown in the time series are $O(100) \times \Delta t$ apart, showing the extremely high spatio-temporal resolution that was employed. We also remark at this point that while the *Ra* values we explore in this model (up to $Ra = 10^4$) may not seem very high to those familiar with Boussinesq fluids, the Nusselt numbers obtained here (up to over 70) correspond to significantly higher Rayleigh numbers in those models. For example at $Ra = 5000$ with the temperature profile shown in figure 1(*a*) the Nusselt number of 40 corresponds to an $O(10^8)$ Rayleigh number for the infinite Prandtl number limit of the Boussinesq equations.

Data for the *Nu* vs. *Ra* relationship from the numerical solution of equations (2.1)–(2.3) are presented in figures 2 and 3. The data points are essentially of two types: asterisks indicate data for which *Ra* was increased from the bifurcation point to $Ra = 10^4$ in a cell of aspect ratio 2 (this run is denoted by $Ra^{\nearrow}$), and stars in figure 3 indicate data for which *Ra* was decreased from a value of $Ra = 1255$ to its bifurcation value (this run will be referred to by $Ra_{\searrow}$). The last data point of the $Ra^{\nearrow}$ run (namely, $Ra = 10^4$) was for a domain of aspect ratio 1 in order to reduce the computation time by a factor of 2 and is indicated with a circle. For this value of *Ra* the dominant dynamical feature of the fluid motion is plume or 'blob' shedding from the thin thermal boundary layers. The plumes traverse the height of the box, having little or no interaction with more horizontally distant plumes, so we expect that the
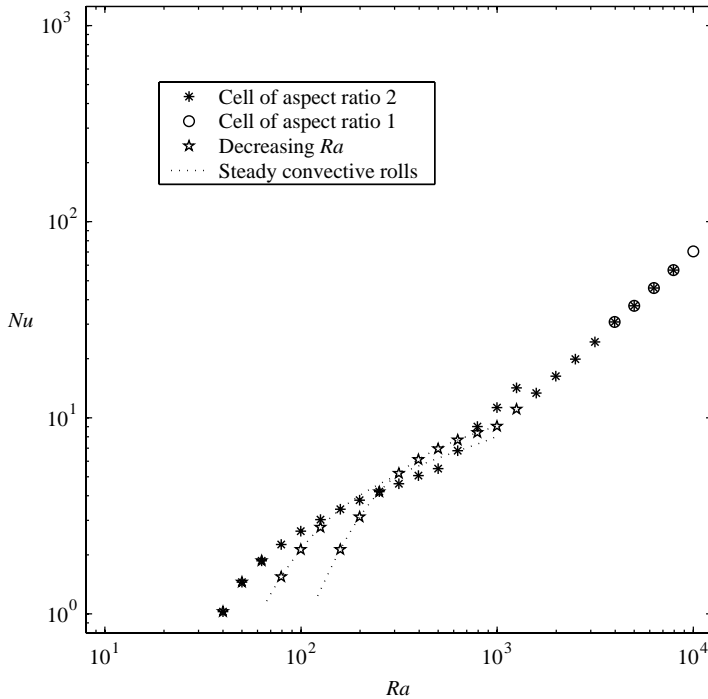
FIGURE 3. The data from the run with increasing Ra is shown together with data for the run in which Ra was decreased from $Ra = 1255$, indicated by stars. The heat transport for the 2-pair and 3-pair steady roll solutions is shown by the dotted line.

average vertical heat transport over half the box should be the same as that over the entire cell. To confirm this we re-computed the numerical solution on a cell of aspect ratio 1 for the four previous highest values of Ra leading up to $Ra = 10^4$. As is seen in figure 2, the heat transport for the aspect ratio 1 solutions (also indicated with circles) agrees with that of the aspect ratio 2 solutions. This aspect ratio independence of Nu at high Ra is distinct from the behaviour of fluid convective turbulence, perhaps due to the lack of a large-scale circulation.

Important features of the Nu vs. Ra data plotted in figure 2 are best discussed with the aid of visual images of the solution for different values of the Rayleigh number. In figure 4 we provide snapshots of the temperature field at various Rayleigh numbers from the $Ra \nearrow$ run. Between onset and $Ra \sim 500$, the simulation shows a pair of steady, nonlinear rolls that simply increase in strength as Ra increases; note that the horizontal periodicity prevents a solution consisting of a single roll in the cell. Solutions in the Ra regime between 500 and 1200 (the beginning of the high-Ra regime) display a rich variety of dynamics that have been studied in considerable detail (Graham & Steen 1994; Cherkaoui & Wilcock 1999). For values of Ra slightly above 500, a secondary instability begins to dominate. The instability appears as a disturbance in the boundary layer that propagates into the vertical components of the roll as can be seen in figure 4(a–c). This new feature of the dynamics is accompanied by a noticeable change in the heat transport properties of the flow. At the point $Ra = 500$, the Nu–Ra curve bends sharply upward and, in the range $500 \lesssim Ra \lesssim 1200$, the curve scales according to $Nu \sim 0.0091 Ra^{1.03}$. The scaling is over a limited range of Ra (about an octave), and it is not very clean there, but at this
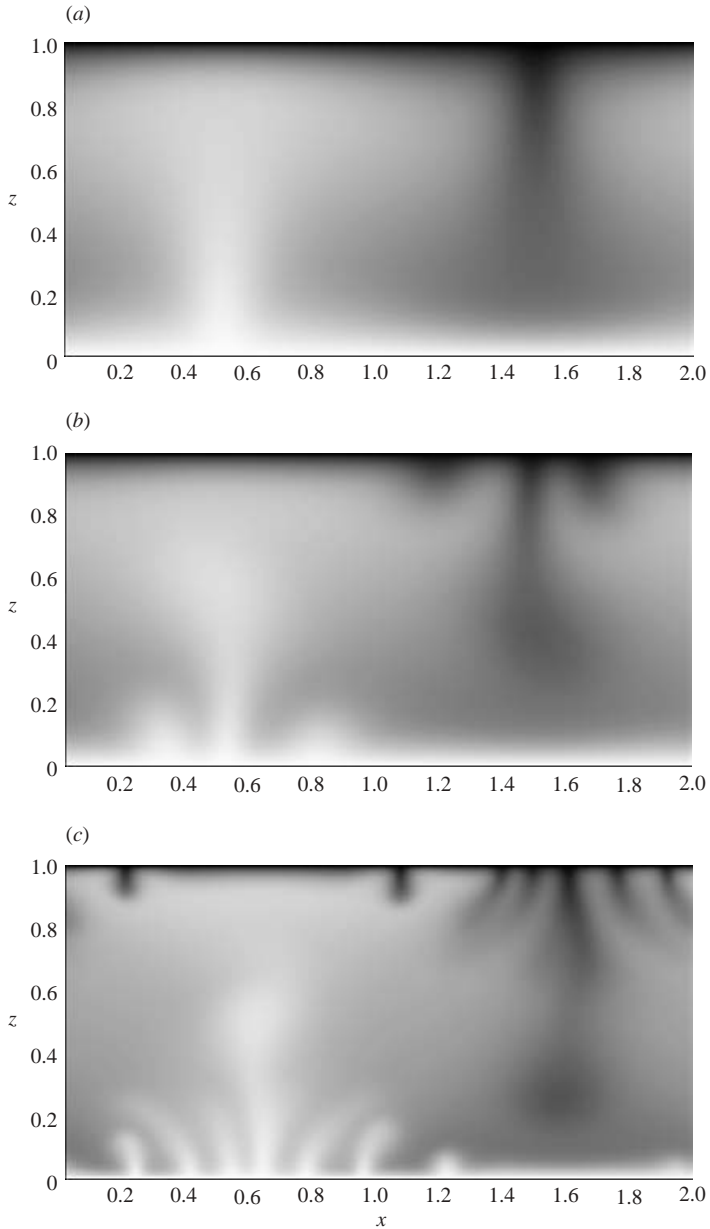
Figure 4(*a*). For caption see facing page.

resolution in *Ra* the heat transport has its largest slope in this region; see Graham & Steen (1994) for further discussion.

Continuing up the $Ra^\nearrow$ run, we observe that between $Ra = 1255$ and $Ra = 1581$ the motion changes rather abruptly from time-dependent rolls to plume shedding, as is evident in figure 4(*d*–*f*). The *Nu*–*Ra* relationship also undergoes an abrupt change over this interval. In fact, it decreases in going from $Ra = 1255$ to $Ra = 1581$ (see figure 2). For values of *Ra* greater than 1581 the fluid motion continues to be dominated by blobs of hot (cold) fluid breaking off the bottom (top) boundary layer
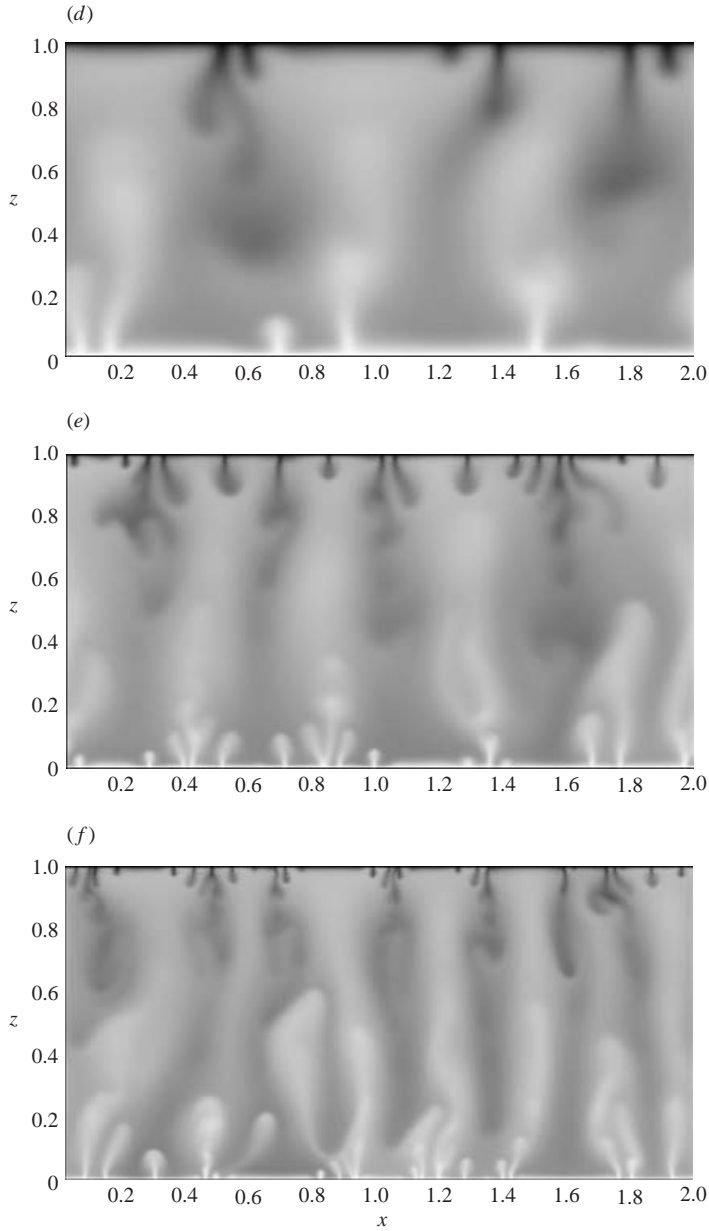
(*d*)

(*e*)

(*f*)

FIGURE 4. Snapshots of the temperature field for (*a*) $Ra = 315$, (*b*) 500, (*c*) 1255, (*d*) 1581, (*e*) 5000, (*f*) 7924.

and drifting upward (downward). We refer to the dynamics in this Rayleigh number regime as 'turbulent', at least in the sense that it is spatially and temporally chaotic (presumably) displaying dynamics over a range of length scales. We also observe a robust 'anomalous' *Nu–Ra* scaling to emerge in this high-*Ra* range. The best fitting power law to the data has an exponent very close 0.9, clearly distinct from the classical $Nu \sim Ra$ scaling law. The anomalous scaling regime we observe is relatively small – on the order of a single decade – and so the deviation from exponent 1 could be

attributed to logarithmic terms or other transient corrections to scaling. It would be necessary to push the Rayleigh number significantly higher to resolve these questions, but we did not go beyond $Ra = 10^4$ in this series of experiments due to computing time restraints.

Hysteretic effects are also present in the dynamics in the Rayleigh number regime ($500 \lesssim Ra \lesssim 1200$). Following the data for the $Ra_\searrow$ run indicated by stars in figure 3, we observed that for decreasing Ra starting with an initial condition in the 'turbulent' state, the solution follows several different branches back down to Ra_c, none of which agree with the solution obtained for increasing Ra. Initially, for Ra values roughly between 1000 and 160, the solution favours three pairs of steady rolls in the 2×1 cell in contrast to the single pair observed on the $Ra_\nearrow$ run. As Ra is reduced from 160 to 100, the solution jumps to two pairs of rolls exhibiting a significant increase in the heat transport. Finally, as Ra is reduced from 79 through 50 or so, the solution switches from two pairs of rolls to the single pair, again with an increase in the heat transport. These steady multiple roll solutions bifurcate off the $Nu = 1$ line at values of Ra higher than $Ra_c = 4\pi^2$, and they are born unstable. However they do enjoy a limited band of stability that the $Ra_\searrow$ run explores; the $Ra_\nearrow$ run bypasses these solutions altogether. These nonlinear, steady roll solutions – be they stable or unstable – were computed numerically by solving the steady equations using Newton's method and their heat transport compared well with those from simulation runs. The heat transport in the directly computed steady flows is shown as the dotted curves in figure 3.

4. Variational (upper) bound on the heat transport

In this section we develop an implementation of the variational 'background field' approach to bounding the heat transport (Doering & Constantin 1996; Nicodemus, Grossmann & Holthaus 1997). This method was recently applied to the model at hand (Doering & Constantin 1998), but the analysis here will produce a better (i.e. lower) bound. The background method produces rigorous limits on the time-averaged bulk transport for any solutions of the equations of motion. It is an alternative to the power integral method for statistically stationary solutions pioneered by Howard (1963) and the multiple boundary layer method introduced by Busse (1969), which has also been applied to porous-medium convection by Busse & Joseph (1972), Gupta & Joseph (1973) and Vitanov (2000). The two techniques are deeply inter-related, as has been established by Kerswell (1998), but in practice the background method is convenient for producing rigorous estimates for high Rayleigh numbers, so we use that technique here.

The background method begins with a functional translation of the temperature field by a 'background field', a time-independent function that carries the inhomogeneous boundary conditions:

$$T(\boldsymbol{x}, t) = \tau(z) + \theta(\boldsymbol{x}, t) \tag{4.1}$$

with

$$\tau(0) = 1, \quad \tau(1) = 0. \tag{4.2}$$

The boundary conditions for τ – which is otherwise arbitrary at this point – force the fluctuations θ to vanish at the top and bottom plates.

The bounds are derived by appropriately combining relevant energy equations. In this case we consider

$$\frac{1}{2}\frac{d}{dt}\|\theta\|^2 = -\|\nabla\theta\|^2 + \int \theta\tau'' - \int \theta w\tau' \tag{4.3}$$

and

$$\|\nabla T\|^2 = \|\nabla\theta\|^2 + 2\int \theta_z\tau' + A\int_0^1 \tau'(z)^2\,dz. \tag{4.4}$$

Taking the long-time average of the linear combination $c\times(4.3) + (4.4)$, where $c > 1$, and using (2.7) gives

$$Nu = \int_0^1 \tau'^2\,dz - \mathscr{F}_\tau[\theta, w] \tag{4.5}$$

where

$$\mathscr{F}_\tau[\theta, w] = \frac{1}{A}\left\langle \int \left((c-1)|\nabla\theta|^2 + c\theta w\tau' + (2-c)\theta\tau''\right)\right\rangle. \tag{4.6}$$

The functional arguments of $\mathscr{F}$ satisfy Dirichlet boundary conditions at $z = 0, 1$. As is typical of many convection models where inertia plays no role, the velocity field is slaved to the temperature field according to a pointwise constraint. Here the constraint is derived from (2.3) by eliminating the pressure:

$$-\Delta w = Ra(D^2 - \Delta)\theta \tag{4.7}$$

where we have introduced the notation $D = d/dz$. The minimum value, $\mathscr{F}_{min}$, of the functional $\mathscr{F}$ over all fields θ and w satisfying homogeneous Dirichlet boundary conditions and the constraint in (4.7) can be computed in terms of the background field; see Doering & Constantin (1998) for the complete details. The expression for $\mathscr{F}_{min}$ is then used in (4.5) to derive the bound

$$Nu \leqslant 1 + \frac{1}{4a(1-a)}\int_0^1 (\tau'+1)^2\,dz, \tag{4.8}$$

where $a = 1 - c^{-1}$ is now a real number which must lie between 0 and 1. To ensure that $\mathscr{F}_{min} > -\infty$ exists, it is necessary to require that the quadratic part of $\mathscr{F}$, namely

$$\mathscr{H}[\theta, w] = \frac{1}{A}\left\langle \int \left(a|\nabla\theta|^2 + \theta w\tau'\right)\right\rangle, \tag{4.9}$$

is positive semi-definite. That is, for any background profile $\tau(z)$ and parameter value $0 < a < 1$ for which $\mathscr{H}[\theta, w]$ is positive semi-definite, the expression on the right-hand side of (4.8) is an upper bound on the Nusselt number.

The positivity constraint for the quadratic form is a spectral constraint for the elliptic operator $\mathscr{L}$ in $\mathscr{H}$, where the eigenvalue problem $\lambda\theta = \mathscr{L}\theta$ is

$$\left.\begin{array}{l} \lambda\theta = -2a\Delta\theta + \tau'w + (D^2 - \Delta)W, \\ 0 = \Delta w + Ra(D^2 - \Delta)\theta, \\ 0 = \Delta W + Ra\tau'\theta, \end{array}\right\} \tag{4.10}$$

introducing $W(\boldsymbol{x})$ as the Lagrange multiplier field for the constraint in (4.7); it satisfies the same boundary conditions as w and θ. The condition $\mathscr{H} \geqslant 0$ is equivalent to $\lambda^0 \geqslant 0$, where λ^0 denotes the lowest eigenvalue of (4.10). Hence we may rewrite the

variational problem as

$$Nu - 1 \leqslant \inf_{0 < a < 1, \ \tau \in \mathscr{S}} \left(\frac{1}{4a(1-a)} \int_0^1 (\tau'(z) + 1)^2 \, \mathrm{d}z \right) \tag{4.11}$$

where

$$\mathscr{S} = \left\{ \tau \ : \ \int_0^1 (\tau'(z) + 1) \, \mathrm{d}z = 0, \ \lambda^0(\tau) \geqslant 0 \right\}. \tag{4.12}$$

We will not compute the absolute minimum bound, as this is both beyond exact analysis and an extremely difficult computational problem.† As an alternative to either a numerical solution to the full variational problem or a less-than-optimal analytical estimate of the optimal bound from above, we take an intermediate approach. We restrict the set of profiles to a one-parameter subset of $\mathscr{S}$ and then optimize over this restricted set. That is, we solve the variational problem:

$$Nu - 1 \leqslant \inf_{0 < a < 1, \ \tau \in \mathscr{T}} \left(\frac{1}{4a(1-a)} \int_0^1 (\tau' + 1)^2 \, \mathrm{d}z \right) \tag{4.13}$$

where

$$\mathscr{T} = \{ \tau_\delta \ : \ \lambda^0(\tau_\delta) \geqslant 0 \} \subset \mathscr{S} \tag{4.14}$$

with λ^0 the lowest eigenvalue of the operator in (4.10) with τ_δ in place of τ. Because the set $\mathscr{T}$ lies within $\mathscr{S}$, the solution to (4.13) provides a bound from above for the solution of the full variational problem (4.11); we refer to it as a 'semi-optimal' bound. The single parameter for the family $\mathscr{T}$ is δ, with $0 < \delta \leqslant \frac{1}{2}$, where the profiles τ_δ are piecewise linear:

$$\tau_\delta(z) = \begin{cases} 1 - \dfrac{z}{2\delta}, & 0 \leqslant z \leqslant \delta \\[2mm] \dfrac{1}{2}, & \delta \leqslant z \leqslant 1 - \delta \\[2mm] \dfrac{1-z}{2\delta}, & 1 - \delta \leqslant z \leqslant 1. \end{cases} \tag{4.15}$$

The piecewise linearity of the τ_δ profiles greatly simplifies the Euler–Lagrange equations in (4.10); they permit exact solution with far more ease than the full variational problem.

The functional to be minimized is

$$\int_0^1 (\tau_\delta' + 1)^2 \, \mathrm{d}z = \left(\frac{1}{2\delta} - 1 \right), \tag{4.16}$$

so δ must be chosen as large as possible, while still satisfying the spectral constraint. A wavenumber naturally enters the problem by virtue of the horizontal periodicity of the fluctuation field θ (and w and W). For (non-dimensional) horizontal periods Λ_x and Λ_y in the x- and y-directions respectively, we Fourier transform the fields

---

† A complete numerical solution to such a background variational problem has only very recently been carried out for the first time – for the case that includes turbulent Couette flow and Rayleigh–Bénard convection in a Boussinesq fluid at finite Prandtl number – by Plasting & Kerswell (2003).

according to

$$f(x, y, z) = \sum_{k} e^{ik \cdot x} f_k(z), \tag{4.17}$$

where now $x = (x, y)$, $k = 2\pi(n/\Lambda_x, m/\Lambda_y)$ for integers n and m. Then the eigenvalue problem in (4.10) becomes (with $k^2 = |k|^2$)

$$\left.\begin{aligned}
\lambda_k \theta_k &= -2a(D^2 - k^2)\theta_k + \tau'_\delta w_k + k^2 W_k, \\
0 &= (D^2 - k^2)w_k + Rak^2\theta_k, \\
0 &= (D^2 - k^2)W_k + Ra\tau'_\delta\theta_k.
\end{aligned}\right\} \tag{4.18}$$

For each wave vector k there is a convex set of background profiles characterized by $\lambda_k^0(\tau) \geqslant 0$ and the corresponding isospectral surface $\lambda_k^0(\tau) = 0$. Because the spectral constraint is imposed mode by mode, we are naturally led to a value of δ for each value of k. From this set of possible values for δ we must choose a single value that ensures the spectral constraint is satisfied for all values of k. It can then be argued from the underlying functional geometry that a strategy for choosing the optimal value of δ is:

> To each value of k, there corresponds a value of δ_k which determines the k-optimal background τ_{δ_k}. The optimal background $\tau_{\delta_{opt}}$ is selected by choosing δ_{opt} to be the minimum of all δ_k, ensuring that $\lambda_k^0(\tau_{\delta_{opt}}) \geqslant 0$ for all wavenumbers.

This is our procedure for solving (4.13). Fix values of a and Ra. For all but finitely many of the k we have $\lambda_k^{gr}(\tau_{1/2}) > 0$. For the remaining k we solve the system of ODEs in (4.18) adjusting δ so that $\lambda_k^{gr}(\tau_\delta) = 0$. (In general, λ may vanish for more than one δ. These other zeros correspond to higher eigenvalues in the spectrum and they necessarily occur for larger values of δ.) In this way we produce a (finite) sequence of δ_k and, as described above, δ_{opt} is precisely the smallest of all the δ_k. Then, keeping Ra fixed, we choose a so as to minimize the value of the bound

$$Nu \leqslant 1 + \frac{1}{4a(1-a)} \int_0^1 (\tau'_\delta + 1)^2 \, dz \tag{4.19}$$

$$= 1 + \frac{1}{4a(1-a)} \left(\frac{1}{2\delta(a, Ra)} - 1 \right). \tag{4.20}$$

The minimization over a produces a single value of δ for a given value of Ra, $\delta = \delta(Ra)$, and then inserting $\delta = \delta(Ra)$ into (4.19) produces the desired bound of Nu in terms of Ra.

Of course, optimizing over the restricted set $\mathscr{T}$ (4.14) will not result in the absolute optimal bound. However, it is reasonable to suspect that the resulting 'semi-optimal' bound will be close to true optimum, perhaps even approaching it in the limit $Ra \to \infty$. Restricting the set of profiles is not the only way to simplify the full optimal problem. In Doering & Constantin (1998) the variational problem was modified by strengthening the constraint slightly (the goal being to eliminate the wavenumber dependence from the optimization problem altogether) and then carrying out the full optimization for the 'new' problem. That result will be used as a benchmark with which we may see the improvement of the new bound to be derived here.

Because τ'_δ is discontinuous, (4.18) with $\lambda_k = 0$ must be solved separately in the three regions $[0, \delta]$, $[\delta, 1-\delta]$, $[1-\delta, 1]$ with the solutions and their first derivatives matched across the boundaries. The end result is a linear problem in 18 variables. The

invariance of the equations under the change of variable $z \to 1 - z$ may be used to show that the lowest eigenfunctions we seek are even about $z = \frac{1}{2}$, so their derivatives vanish there. This symmetry reduces the domain for our problem to only two regions, say region I $= [0, \delta]$ and region II $= [\delta, \frac{1}{2}]$, and hence to a problem of 12 variables with boundary conditions:

  (i) homogeneous Dirichlet boundary conditions at $z = 0$;
  (ii) solutions and their first derivatives are continuous at $z = \delta$;
  (iii) homogeneous Neumann boundary conditions at $z = \frac{1}{2}$.

Hence in region I $= [0, \delta]$ the solution is

$$\left.\begin{aligned}
\theta_k &= A_1 \sinh(p_1 z) + A_2 \sinh(p_2 z), \\
w_k &= -\frac{Rak^2}{\Gamma}(A_1 \sinh(p_1 z) - A_2 \sinh(p_2 z)) + A_3 \sinh(kz), \\
W_k &= \frac{Ra}{2\delta\Gamma}(A_1 \sinh(p_1 z) - A_2 \sinh(p_2 z)) + \frac{1}{2\delta k^2} A_3 \sinh(kz),
\end{aligned}\right\} \quad (4.21)$$

where $\Gamma = \sqrt{Rak^2/2a\delta}$, $p_1 = \sqrt{k^2 + \Gamma}$, $p_2 = \sqrt{k^2 - \Gamma}$, and the undetermined constants are A_1, A_2, A_3. And in region II $= [\delta, \frac{1}{2}]$, using $\zeta = z - \frac{1}{2}$, the solution is

$$\left.\begin{aligned}
\theta_k &= \alpha_1 \cosh(k\zeta) + \alpha_2 \zeta \sinh(k\zeta), \\
w_k &= -\alpha_1 \frac{Rak}{2} \zeta \sinh(k\zeta) + \alpha_2 \frac{Ra}{4}(\zeta \sinh(k\zeta) - k\zeta^2 \cosh(k\zeta)) + \alpha_3 \cosh(k\zeta), \\
W_k &= \frac{4a}{k} \alpha_2 \cosh(k\zeta),
\end{aligned}\right\} \quad (4.22)$$

where α_1, α_2, α_3 are the undetermined constants.

The boundary conditions at $z = 0$ and $z = \frac{1}{2}$ have already been imposed, which explains why there are only six undetermined coefficients above. Imposing the remaining six matching conditions at $z = \delta$, we obtain a sixth-order homogeneous linear system in the unknowns A_1, A_2, A_3, α_1, α_2, α_3. In order to obtain a solution, the matrix of coefficients, which depends on a, Ra, k and δ, must have a vanishing determinant. Adjusting δ to ensure that the determinant does vanish produces the value of δ_k for each k and fixed Ra and a. Once the values of δ_k for the relevant k have been found, we must choose the smallest one to ensure that the spectral constraint is satisfied for all k. This gives us a value of δ for the given values of a and Ra. Next we minimize the bound in (4.8) over a, thus producing a value of δ for each value of Ra. Inserting the relation $\delta = \delta(Ra)$ into (4.8) provides an upper bound for Nu in terms of Ra. The result is shown in figure 5.

We first observe that the numerical bound bifurcates from the proper value $Ra_c = 4\pi^2$; this is one of the benefits of using the balance parameter a, first introduced in the context of shear flow by Nicodemus *et al.* (1997). On the other hand, this bound significantly overestimates the heat transport for values of Ra just above Ra_c. The reason for that is that for such low values of Ra a piecewise linear profile like τ_δ that is flat in the middle is not a very good approximation of the optimal temperature profile, which is a smooth perturbation of the linear conduction profile. In any case, for Ra values larger than roughly 200, the bound exhibits a very definite scaling according to $Nu \sim 0.0297 Ra$, representing a 15% prefactor improvement in the asymptotic bound $Nu \lesssim \frac{9}{256} Ra \approx 0.0325 Ra$ derived in Doering & Constantin (1998).
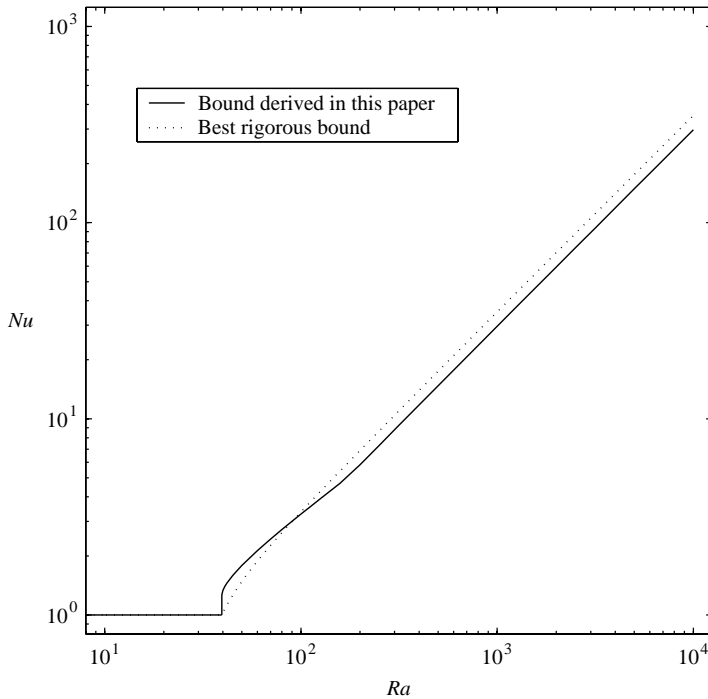
FIGURE 5. The bound derived in this paper is indicated by the solid line. It is extremely well-fitted by the formula $Nu = 0.0297Ra$ for $Ra > 250$. The dotted line is the previous best rigorous bound ($Nu \sim 0.0352Ra$ asymptotically for large Ra) obtained in Doering & Constantin (1998). The minimum of these two curves is now the best bound.

5. Conclusions

We have presented the results of a detailed, highly resolved set of numerical experiments on a model of convection in a fluid-saturated porous layer along with measurements of the heat transport. We observe that as the Rayleigh number is increased adiabatically, the flow passes from a steady state to more complex dynamical states. The complex dynamics comes in two general varieties. One is time dependent (temporally periodic or perhaps chaotic) but with the spatial structure of the flow still being dominated by the single pair of rolls created at onset. The heat transport in this state is reasonably well-described by the classical $Nu \sim Ra$ scaling. The other mode of convection, appearing at high Rayleigh number, is a state where the long-range spatial coherence is lost and what might be characterized as a 'turbulence' sets in. The dynamics is dominated by blobs of hot (cold) fluid breaking away from the bottom (top) boundary layer and convecting across the layer. No large-scale flow appears, as is seen in the hard-turbulence regime of fluid convection, but the Nusselt number scaling decreases in analogy with that transition. In this turbulent state of convection in the porous layer model, the heat transport is better described by a $Nu \sim Ra^{0.9}$ fit, and this scaling is quite robust over nearly an entire decade of Ra. It is not clear if this correction to the classical scaling really is an exponent change, or if there are logarithmic corrections, or if it is a transient deviation that will ultimately revert back to a $Nu \sim Ra$ behaviour.

It is worthwhile to discuss a unique feature of porous-medium heat transport Nu–Ra scaling in this regard. For regular convection, the so-called classical 1/3 scaling

results from assuming that the thermal boundary layer adjusts its thickness so as to be marginally stable to convection within itself (Howard 1964; Doering & Constantin 1998). The same exponent also results from the assumption that there is finite heat flux into a semi-infinite layer. In either case, the exponent is a consequence of the fact that the layer thickness h enters the Rayleigh number as h^3. For convection in a porous layer, the same arguments suggest scaling with exponent 1 because h enters the Rayleigh number linearly, the other two powers of length being supplied by the square of the (small) pore length scale in the Darcy permeability coefficient K.

The so-called 'ultimate' scaling for fluid convection with a 1/2 exponent results from various assumptions. It was originally derived (with logarithmic corrections) from a statistical closure theory by Kraichnan (1962). As pointed out by Spiegel (1971), it also follows from the assumption, in the spirit of Kolmogorov, that a 'residual' transport remains even in the limit of vanishing microscopic transport coefficients. That is, $Nu \sim (PrRa)^{1/2}$ is the only possibility if the physical heat flux is finite and non-vanishing in the limit of vanishing thermal conduction and fluid viscosity.† For convection in a porous layer, the same argument – that the physical heat flux becomes independent of the thermal conduction coefficient at high Ra – suggests scaling with exponent 1, the same as the classical exponent. Hence in the problem at hand, a crossover to a different exponent as Ra increases indefinitely might not be expected. Although it appears to be a reliable result from the simulations reported here, we do not know the physical source of the 'anomalous' scaling with the exponent ≈ 0.9 observed at the highest Rayleigh numbers. Hence we cannot predict whether or not this is a transient state and if the 'classical-ultimate' $Nu \sim Ra^1$ scaling will eventually reappear.

We also derived new and improved upper limits for the Nusselt number as a function of the Rayleigh number. At high Rayleigh numbers the bounds display the classical scaling with an explicit prefactor: $Nu \leqslant 0.0297 \times Ra$. In order to compare the numerical upper bound with the simulation data, we plot the heat transport for the simulations and our hybrid analytical/numerical bound on the same graph in figure 6. This plot also includes simulation data from Graham & Steen (1994) (indicated by squares) as well as data (indicated with plus signs) from another increasing Ra simulation run using a completely different numerical scheme (Kurganov, Noelle & Petrova 2001) than that discussed in §3. All of these simulations produce solutions that agree extremely well in their heat transport properties. In the intermediate Ra range where the classical scaling is observed, the upper bound is less than a factor of 2 above the data. At its worst at $Ra = 10^4$, the numerical bound (valid in two or three dimensions) is about a factor of 4 above the (two-dimensional) simulation data. It appears from the plot that the simulation is drifting away from the bound as the highest Ra data apparently scales with an exponent slightly less than unity.

Not unexpectedly, we cannot rule out the possibility that the rigorous upper bounds may be improved. An exact solution of the variational problem, akin to the recent analysis for fluid convection by Plasting & Kerswell (2003), would probably produce some further improvement, at least in the prefactor. But it is not possible to predict if a correction to the classical-ultimate scaling is to be found in the optimal bound. A recent application of Busse's multiple boundary layer analysis via Howard's

---

† Kraichnan's theory and the Kolmogorov–Spiegel argument predict different Prandtl number dependences, while the rigorous upper bounds $\sim Ra^{1/2}$ are uniform in the Prandtl number.
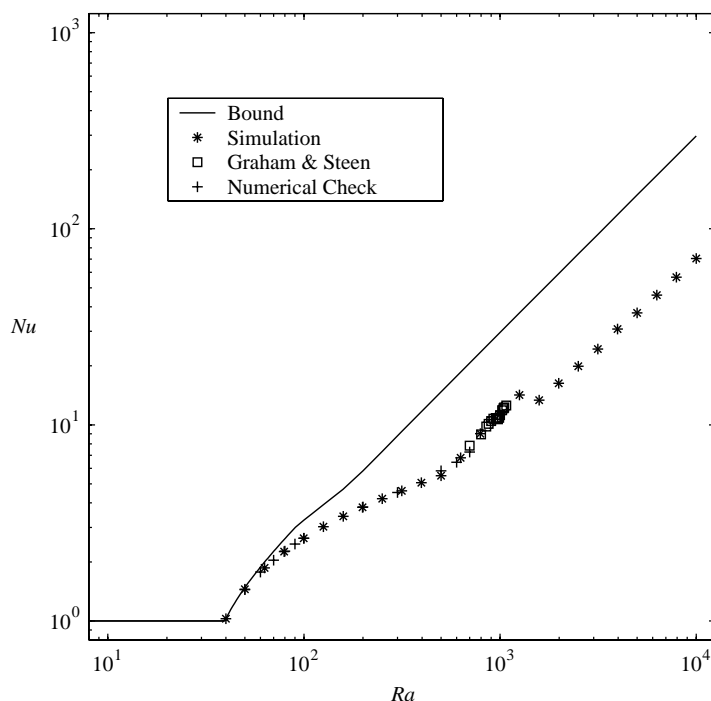
FIGURE 6. Lower envelope of the bounds displayed in figure 5 (solid line) together with the data from the numerical simulations. The heat transport data from (Graham & Steen 1994) are included (squares) as well. Also shown are data from another increasing Ra simulation using a completely different numerical scheme and run protocol (indicated +).

statistically steady power integral method by Vitanov (2000) suggests that such an approach may help to settle this question, but we are not yet able to extract the high-Rayleigh-number behaviour of the bound from that theory.

It is evident that high-Rayleigh-number convection in a fluid-saturated porous layer displays a rich range of dynamics with curious heat transport properties. Although at high Rayleigh numbers this model is difficult to realize reliably in laboratory experiments, it is attractively accessible to both computation and analysis. And further understanding of the processes determining the heat transport in this relatively simple system is likely to shed light on the more complicated – and more widely applicable – problem of high-Rayleigh-number turbulent convection in Boussinesq fluids.

REFERENCES

BUSSE, F. 1969 On Howard's upper bound for heat transport by turbulent convection. *J. Fluid Mech.* **37**, 457–477.

BUSSE, F. & JOSEPH, D. 1972 Bounds for heat transport in a porous layer. *J. Fluid Mech.* **54**, 521–543.

CHAN, S.-K. 1971 Infinite Prandtl number turbulent convection. *Stud. Appl. Maths* **50**, 13–49.

CHAVANNE, X., CHILLA, F., CASTAING, B., HEBRAL, B., CHABAUD, B. & CHAUSSY, J. 1997 Observation of the ultimate regime in Rayleigh-Bénard convection. *Phys. Rev. Lett.* **79**, 3648–3651.

CHERKAOUI, A. S. M. & WILCOCK, W. S. D. 1999 Characteristics of high Rayleigh number two-dimensional convection in an open-top porous layer heated from below. *J. Fluid Mech.* **394**, 241–260.

CONSTANTIN, P. & DOERING, C. R. 1999 Infinite Prandtl number convection. *J. Statist. Phys.* **94** (1-2), 159–172.

DOERING, C. R. & CONSTANTIN, P. 1996 Variational bounds on energy dissipation in incompressible flows. III. Convection. *Phys. Rev.* E **53**, 5957–5981.

DOERING, C. R. & CONSTANTIN, P. 1998 Bounds for heat transport in a porous layer. *J. Fluid Mech.* **376**, 263–296.

DOERING, C. R. & CONSTANTIN, P. 2001 On upper bounds for infinite Prandtl number convection with or without rotation. *J. Math. Phys.* **42** (2), 784–795.

GLAZIER, J., SEGAWA, T., NAERT, A. & SANO, M. 1999 Evidence against ultrahard thermal turbulence at very high Rayleigh numbers. *Nature* **398**, 307–310.

GRAHAM, M. D. & STEEN, P. H. 1994 Plume formation and resonant bifurcations in porous-media convection. *J. Fluid Mech.* **272**, 67–89.

GROSSMANN, S. & LOHSE, D. 2000 Scaling in thermal convection: a unifying theory. *J. Fluid Mech.* **407**, 27–56.

GUPTA, V. & JOSEPH, D. 1973 Bounds for heat transport in a porous layer. *J. Fluid Mech.* **57**, 491–514.

HESLOT, F., CASTAING, B. & LIBCHABER, A. 1987 Transitions to turbulence in helium gas. *Phys. Rev.* A **36**, 5870–5873.

HOWARD, L. N. 1963 Heat transport by turbulent convection. *J. Fluid Mech.* **17**, 405–432.

HOWARD, L. N. 1964 Convection at high Rayleigh numbers. In *Applied Mechanics, Proc. 11th Congress of Applied Mathematics* (ed. H. Görtler), pp. 1109–1115.

KADANOFF, L. 2001 Turbulent heat flow: Structures and scaling. *Physics Today* **54**, 34.

KERR, R. & HERRING, J. 2000 Prandtl number dependence of Nusselt number in direct numerical simulations. *J. Fluid Mech.* **419**, 325–344.

KERSWELL, R. R. 1998 Unification of variational principles for turbulent flows: the background method of Doering-Constantin and the mean-fluctuation formulation of Howard-Busse. *Physica* D **121**, 175–192.

KRAICHNAN, R. H. 1962 Turbulent thermal convection at arbitrary Prandtl number. *Phys. Fluids* **5**, 1374–1389.

KURGANOV, A., NOELLE, S. & PETROVA, G. 2001 Semi-discrete central-upwind schemes for hyperbolic conservation laws and Hamilton-Jacobi equations. *SIAM J. Sci. Comput.* **23**, 707–740.

LISTER, C. 1990 An explanation for the multivalued heat transport found experimentally for convection in a porous medium. *J. Fluid Mech.* **214**, 287–320.

NICODEMUS, R., GROSSMANN, S. & HOLTHAUS, M. 1997 Improved variational principle for bounds on energy dissipation in turbulent shear flow. *Physica* D **101** (1-2), 178–190.

NICODEMUS, R., GROSSMANN, S. & HOLTHAUS, M. 1998 The background flow method. Part 1. Constructive approach to bounds on energy dissipation. *J. Fluid Mech.* **363**, 281–300.

NIELD, D. & JOSEPH, D. 1985 Effects of quadratic drag on convection in a saturated porous medium. *Phys. Fluids* **28**, 995–997.

NIELD, D. A. & BEJAN, A. 1992 *Convection in Porous Media*. Springer.

NIEMELA, J., SKRBEK, L., SREENIVASAN, K. & DONNELLY, R. 2000 Turbulent convection at very high Rayleigh numbers. *Nature* **404**, 837–840.

OTERO, J. 2002 Bounds for the heat transport in turbulent convection. PhD thesis, University of Michigan.

OTERO, J., WITTENBERG, R. W., WORTHING, R. A. & DOERING, C. R. 2002 Bounds on Rayleigh-Bénard convection with an imposed heat flux. *J. Fluid Mech.* **473**, 191–199.

PLASTING, S. C. & KERSWELL, R. R. 2003 Improved upper bound on the energy dissipation rate in plane Couette flow: The full solution to Busse's problem and the Doering–Constantin problem with one-dimensional background field. *J. Fluid Mech.* **477**, 363–379.

SHATTUCK, M., BEHRINGER, R., JOHNSON, G. & GEORGIADIS, J. 1997 Convection and flow in a porous media. Part 1. Visualization by magnetic resonance imaging. *J. Fluid Mech.* **332**, 215–245.

Sᴏᴍᴍᴇʀɪᴀ, J. 1999 Evidence against 'ultrahard' turbulence at very high Rayleigh numbers. *Nature* **398**, 294–295.

Sᴘɪᴇɢᴇʟ, E. 1971 Convection in stars I. Basic Boussinesq convection. *Annu. Rev. Astron. Astr.* **9**, 323.

Vɪᴛᴀɴᴏᴠ, N. K. 2000 Upper bounds on the heat transport in a porous layer. *Physica* D **136**, 322–339.

Xᴜ, X., Bᴀᴊᴀᴊ, K. & Aʜʟᴇʀs, G. 2000 Heat transport in turbulent Rayleigh-Bénard convection. *Phys. Rev. Lett.* **84**, 4357–4360.